Publ. Astron. Soc. Japan (2016) 68 (5), 74 (1–16)
doi: 10.1093/pasj/psw045
Advance Access Publication Date: 2016 May 23

The Hitachi and Takahagi 32 m radio telescopes: Upgrade of the antennas from satellite communication to radio astronomy

Yoshinori Yonekura,[1,*] Yu Saito,[1] Koichiro Sugiyama,[1] Kang Lou Soon,[2] Munetake Momose,[2] Masayoshi Yokosawa,[2] Hideo Ogawa,[3] Kimihiro Kimura,[3] Yasuhiro Abe,[3] Atsushi Nishimura,[3,†] Yutaka Hasegawa,[3] Kenta Fujisawa,[4,5] Tomoaki Ohyama,[6] Yusuke Kono,[6] Yusuke Miyamoto,[1,‡] Satoko Sawada-Satoh,[1] Hideyuki Kobayashi,[7] Noriyuki Kawaguchi,[7] Mareki Honma,[6,8] Katsunori M. Shibata,[7] Katsuhisa Sato,[6] Yuji Ueno,[6] Takaaki Jike,[6] Yoshiaki Tamura,[6,8] Tomoya Hirota,[7,8] Atsushi Miyazaki,[9,§] Kotaro Niinuma,[5,‖] Kazuo Sorai,[10] Hiroshi Takaba,[11] Kazuya Hachisuka,[4,#] Tetsuro Kondo,[12] Mamoru Sekido,[12] Yasuhiro Murata,[13,14] Naomasa Nakai,[15,16] and Toshihiro Omodaka[17]

[1]Center for Astronomy, Ibaraki University, 2-1-1 Bunkyo, Mito, Ibaraki 310-8512, Japan
[2]College of Science, Ibaraki University, 2-1-1 Bunkyo, Mito, Ibaraki 310-8512, Japan
[3]Department of Physical Science, Osaka Prefecture University, 1-1 Gakuen-cho, Naka-ku, Sakai, Osaka 599-8531, Japan
[4]The Research Institute for Time Studies, Yamaguchi University, 1677-1 Yoshida, Yamaguchi, Yamaguchi 753-8511, Japan
[5]Graduate School of Science and Engineering, Yamaguchi University, 1677-1 Yoshida, Yamaguchi, Yamaguchi 753-8512, Japan
[6]Mizusawa VLBI Observatory, National Astronomical Observatory of Japan (NAOJ), 2-12 Hoshigaoka-cho, Mizusawa-ku, Oshu, Iwate 023-0861, Japan
[7]Mizusawa VLBI Observatory, NAOJ, 2-21-1 Osawa, Mitaka, Tokyo 181-8588, Japan
[8]Department of Astronomical Science, SOKENDAI (The Graduate University for Advanced Studies), 2-21-1 Osawa, Mitaka, Tokyo 181-8588, Japan
[9]Korea Astronomy and Space Science Institute, 776 Daedeokdae-ro, Yuseong-gu, Daejeon 305-348, Republic of Korea
[10]Department of Physics/Department of Cosmosciences, Hokkaido University, Kita 10 Nishi 8, Kita-ku, Sapporo, Hokkaido 060-0810, Japan
[11]Faculty of Engineering, Gifu University, 1-1 Yanagido, Gifu, Gifu 501-1193, Japan
[12]Kashima Space Technology Center, National Institute of Information and Communications Technology, 893-1 Hirai, Kashima, Ibaraki 314-8501
[13]Institute of Space and Astronautical Science, Japan Aerospace Exploration Agency, 3-1-1 Yoshinodai, Chuo-ku, Sagamihara, Kanagawa 252-5210, Japan
[14]Department of Space and Astronautical Science, SOKENDAI (The Graduate University for Advanced Studies), 3-1-1 Yoshinodai, Chuo-ku, Sagamihara, Kanagawa 252-5210, Japan
[15]Division of Physics, Faculty of Pure and Applied Sciences, University of Tsukuba, 1-1-1 Tennodai, Tsukuba, Ibaraki 305-8571, Japan

[16]Center for Integrated Research in Fundamental Science and Technology (CiRfSE), University of Tsukuba, 1-1-1 Tennodai, Tsukuba, Ibaraki 305-8571, Japan
[17]Department of Physics and Astronomy, Graduate School of Science and Engineering, Kagoshima University, 1-21-35 Korimoto, Kagoshima, Kagoshima 890-0065, Japan

*E-mail: yoshinori.yonekura.sci@vc.ibaraki.ac.jp
†Present address: Department of Astrophysics, Nagoya University, Furo-cho, Chikusa-ku, Nagoya, Aichi 464-8602, Japan.
‡Present address: Nobeyama Radio Observatory, NAOJ, 462-2 Nobeyama, Minamimaki, Nagano 384-1305, Japan.
§Present address: National Astronomical Observatory of Japan, 2-21-1 Osawa, Mitaka, Tokyo 181-8588, Japan.
‖Present address: Graduate School of Sciences and Technology for Innovation, Yamaguchi University, 1677-1 Yoshida, Yamaguchi, Yamaguchi 753-8512, Japan.
#Present address: Mizusawa VLBI Observatory, NAOJ, 2-12 Hoshigaoka-cho, Mizusawa-ku, Oshu, Iwate 023-0861, Japan.

Received 2016 March 1; Accepted 2016 April 4

Abstract

The Hitachi and Takahagi 32 m radio telescopes (former satellite communication antennas) were so upgraded as to work at 6, 8, and 22 GHz. We developed the receiver systems, IF systems, back-end systems (including samplers and recorders), and reference systems. We measured the performance of the antennas. The system temperature including the atmosphere toward the zenith, T^*_{sys}, is measured to be ∼30–40 K for 6 GHz and ∼25–35 K for 8 GHz. T^*_{sys} for 22 GHz is measured to be ∼40–100 K in winter and ∼150–500 K in summer seasons, respectively. The aperture efficiency is 55%–75% for Hitachi at 6 GHz and 8 GHz, and 55%–65% for Takahagi at 8 GHz. The beam sizes at 6 GHz and 8 GHz are ∼4.′6 and ∼3.′8, respectively. The side-lobe level is less than 3%–4% at 6 and 8 GHz. Pointing accuracy was measured to be better than ∼0.′3 for Hitachi and ∼0.′6 for Takahagi. We succeeded in VLBI observations in 2010 August, indicating good performance of the antenna. We started single-dish monitoring observations of 6.7 GHz methanol maser sources in 2012 December, and found several new sources showing short-term periodic variation of the flux density.

Key words: instrumentation: detectors — instrumentation: interferometers — masers — radio continuum: general — radio lines: general

1 Introduction

Observations with a high angular resolution are crucial in exploring the nature of the universe. At present, a Very Long Baseline Interferometer (VLBI) is the only equipment that can achieve a resolution equal to, or better than, 10 mas. However, only sources with extremely high brightness can be detected by VLBI observations even through the sparse arrangement of antennas. Thus, a large antenna with a high-sensitivity receiver is needed to improve the sensitivity.

In Japan, there is a network called the Japanese VLBI network (JVN), which consists of the following antennas: VERA 20 m (Mizusawa, Iriki, Ogasawara, and Ishigaki), Yamaguchi 32 m, Tsukuba 32 m, Kashima 34 m, Usuda 64 m, Tomakomai 11 m, and Gifu 11 m. For observations at 6.7 GHz, which corresponds to the rest frequency of the methanol maser, four VERA antennas and Yamaguchi 32 m were mainly used for observations before 2010, although the sensitivity and the UV coverage were insufficient.

The Takahagi and Hitachi 32 m antennas, which had been used for satellite communications at 4 and 6 GHz by KDDI, were decommissioned in 2007 March. These antennas were handed over to the National Astronomical Observatory of Japan (NAOJ) on 2009 January 31, and now belong to the Ibaraki station, which is a branch of the Mizusawa VLBI Observatory of NAOJ. NAOJ and Ibaraki University, in cooperation with various universities (Hokkaido University, University of Tsukuba, Gifu University, Osaka Prefecture University, Yamaguchi University, and Kagoshima University), the Geospatial Information Authority of Japan (GSI), the Japan Aerospace Exploration Agency (JAXA), and the National Institute of Information and Communications Technology (NICT), have decided

to use these antennas for a Japanese and East-Asia VLBI network. We will also use these antennas for single-dish and two-element interferometric observations as well as VLBI.

We started the development (conversion from telecommunication antennas to radio telescopes) in 2009. The first scientific VLBI observations were successfully carried out in 2010 August by using the Hitachi antenna. From 2012 December, we started daily observations of 6.7 GHz methanol maser sources in single-dish mode using the Hitachi antenna. The development was almost finished in 2013 December except for the two-element interferometer mode.

In section 2, we describe the development. In section 3, the measured performance for the antennas is described. In section 4, the scientific results are shown. In section 5, we summarize the paper.

Fig. 1. Photograph of Takahagi (front) and Hitachi (back) 32 m antennas. (Color online)

2 Development

2.1 Antenna

The mechanics and surface of the antenna were not changed. The Hitachi antenna was constructed in 1983 and the Takahagi antenna was constructed in 1992 by the Mitsubishi Electric corporation. The design of the Hitachi and Takahagi antennas is of the shaped Cassegrain type, achieving high efficiency, low noise, and low side-lobe levels. These two antennas have the same optics.

The diameter of each antenna is 32 m. Surface accuracy was designed so as to be better than 0.64 mm RMS at night without wind at the particular elevation angles of 35° for Hitachi and 33° for Takahagi, where the stationary satellite that was the target of the antenna when used as a telecommunication antenna is located, and better than 1.6 mm RMS at any elevation angle. The surface accuracies, measured by theodolite, were 0.555, 0.414, and 1.07 mm at elevation angles of 0°, 35°, and 90° in 1983 for Hitachi, and 0.443 and 0.889 mm at elevation angles of 33° and 90° in 1992 for Takahagi. The main dish is composed of 342 aluminum panels. The subreflector has a diameter of 2.9 m and its surface accuracy is better than 0.2 mm RMS.

Four mirrors are used to guide the received signal to the feed horn in the receiver cabin, where the receiver cabin is stable for both azimuth and elevation movements. The receiver and the feed horn are fixed on the ground, whereas the four mirrors rotate with the antenna. In order to achieve good cross-polarization characteristics, three curved mirrors and one plane mirror are used: M1 (nearest to the horn) is a hyperboloid with an effective aperture of 2.0 m;

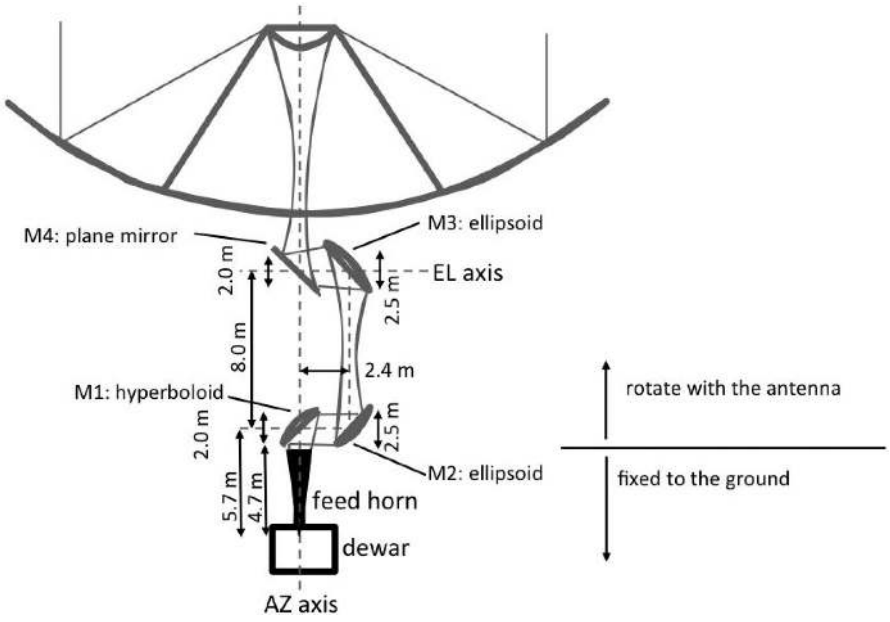

Fig. 2. Optics of the Hitachi and Takahagi 32 m antennas.

Fig. 3. Photograph of the feed horn. By exchanging the bottom of the feed horn, we can change the observation band. (Color online)

M2 and M3 are ellipsoids with an effective aperture of 2.5 m; M4 is a plane mirror with an effective aperture of 2.0 m. The optics of the Hitachi and Takahagi antennas are shown in figure 2. The surface accuracies of these four mirrors are better than 0.2 mm RMS.

The feed horn was newly designed and installed. By exchanging the bottom of the horn, we can change the observation band from the low-frequency band (6.7 and 8 GHz) to the high-frequency band (22 GHz) and vice versa (figure 3).

Two DC motors are used for azimuth (Az) control and two other for elevation (El), in order to reduce backlash. The angular velocity of the antenna is controlled by the applied voltage, which is determined from the difference between the target position and the present position of the antenna. The maximum angular velocity of the Hitachi antenna is $0.^{\circ}3\ s^{-1}$ and that of the Takahagi antenna is $0.^{\circ}1\ s^{-1}$. The maximum angular accelerations are $0.^{\circ}3\ s^{-2}$ and $0.^{\circ}1\ s^{-2}$ for the Hitachi and Takahagi antennas.

The physical ranges of motion is limited to $0^{\circ} \leq Az \leq +360^{\circ}$ (north is 0° and the angle increases for clockwise rotation) and $0.^{\circ}5 \leq El \leq 90.^{\circ}5$ for the Hitachi antenna and $10^{\circ} \leq Az \leq 350^{\circ}$ and $1.^{\circ}5 \leq El \leq 90.^{\circ}5$ for the Takahagi antenna. For safety, we limit the ranges of motion when controlled by PC to be $2^{\circ} \leq Az \leq 358^{\circ}$ and $5^{\circ} \leq El \leq 88^{\circ}$ for the Hitachi antenna and $11^{\circ} \leq Az \leq 349^{\circ}$ and $5^{\circ} \leq El \leq 88^{\circ}$ for the Takahagi antenna.

2.2 Receiver system

We have developed two receiver systems: one is the low-frequency-band receiver system (6.3–7.0 GHz and 8.0–8.8 GHz) and the other is the high-frequency-band receiver system (21–25 GHz) for each antenna. For each receiver system, the components are stored within the dewar, cooled to ~10 K by a cryo-cooler (Suzuki-Shokan RF273S). The receiver system is directly connected to the bottom of the feed horn (figure 3), whose output is in the form of a circular waveguide.

Each receiver system is composed of thermal insulation, a circular waveguide, circular to square transition, polarizer, waveguide to coaxial cable transition (for the low-frequency-band receiver only), and low-noise amplifiers. The output of the receiver dewar is in the form of two coaxial connectors (SMA female connectors for the low-frequency-band receiver, and K female connectors for the high-frequency-band receiver). For the low-frequency-band and high-frequency-band receiver systems, Caltech CITCRYO 4-12A and Nitsuki 9837K low-noise amplifiers are used, respectively (figure 4).

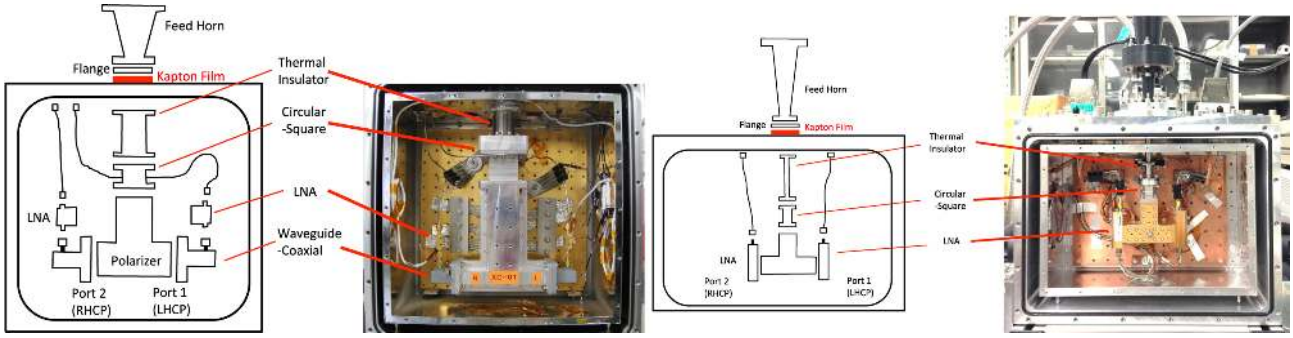

Fig. 4. (Left) Block diagram and a photograph of the low-frequency-band (6–9 GHz) receiver. (Right) Block diagram and a photograph of the high-frequency-band (21–25 GHz) receiver. (Color online)

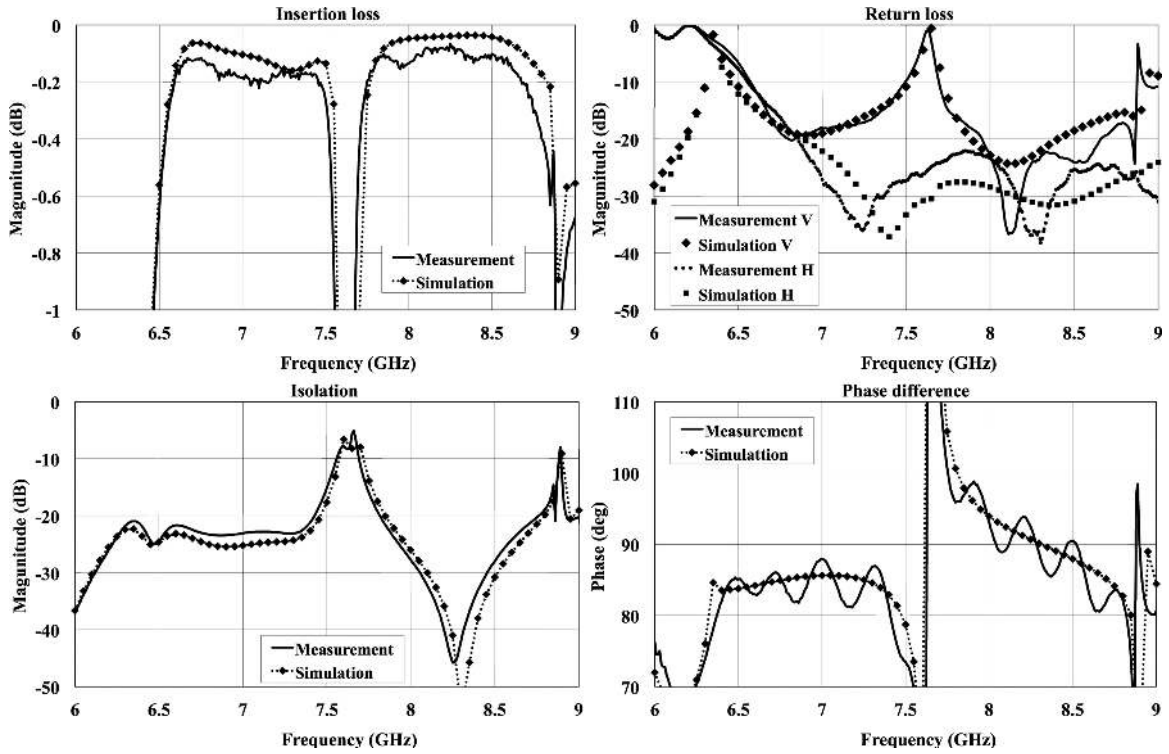

Fig. 5. Electric characteristics of the polarizer for the low-frequency-band receiver. Simulated and measured values of (top left) insertion loss, (top right) return loss, (bottom left) isolation, and (bottom right) phase difference are shown.

We have two target frequency ranges for the low-frequency-band receiver: 6.3–7.0 GHz and 8.0–8.8 GHz. The fractional bandwidth becomes larger than 30% if 6.3–8.8 GHz is covered by one polarizer (2.5 GHz bandwidth at the center frequency of 7.5 GHz). Since the typical achievable fractional bandwidth is ∼20% (e.g., Chen & Tsandoulas 1973; Cresci et al. 2002), we developed a polarizer with good performance at 6.3–7.0 GHz and 8.0–8.8 GHz but with relatively poor performance at 7.0–8.0 GHz by setting the resonance frequency at ∼7.5 GHz. The simulated and measured performance value of the polarizer are shown in figure 5. Target values were insertion loss better than 0.2 dB, return loss better than 20 dB, isolation better than 20 dB, and phase difference $90^\circ \pm 5^\circ$, and these parameters have been achieved. For the high-frequency-band receivers, we have developed a polarizer covering 20.5–25 GHz. We obtained the following performance: insertion loss 0.15 dB on average, return loss better than 20 dB, and isolation better than 20 dB (Kaiden et al. 2010).

The observation bands can be changed by physically exchanging the receiver system and the bottom of the feed horn. It takes ∼3 d to exchange observation bands from low frequency to high frequency and vice versa. On the other hand, the two target frequency ranges for the low-frequency band, i.e., 6.3–7.0 GHz and 8.0–8.8 GHz, can be switched within 10 min by changing the intermediate frequency (IF) setting (see subsection 2.3).

2.3 IF systems

At the receiver cabin of the Hitachi antenna, two orthogonal polarization (left- and right-handed circular polarization, or LHCP and RHCP) outputs of the low-frequency-band receiver of 6.3–8.8 GHz were connected to one of the following two chains, which can be switched: one having a 6.3–7.0 GHz (C-band) band-pass filter and the other having an 8.0–8.8 GHz (X-band) band-pass filter. The LHCP signal is mainly used for observations at 6.3–7.0 GHz, and the RHCP signal is for observations at 8.0–8.8 GHz. Then the signals are down-converted to 0.5–1.0 GHz with the local frequencies of 6088 MHz for C-band and 7680 MHz for X-band. For LHCP, a notch filter to block radio-frequency interference at 6730–6740 MHz (IF frequency of 642–652 MHz) is inserted. IF signals of both polarizations are divided into two outputs; one is connected to the samplers of the two-element interferometer (details will be described in a separate paper), and the other is sent to the observation room. At the observation room, the signal is further divided into four outputs: one is connected to the selector for the input of the sampler (ADS-1000+) for VLBI observation, and the three others are connected to the base-band converter (Nitsuki). The outputs of the base-band converter, having frequency ranges of 0–32 MHz, are connected to samplers (K5/VSSP32) for single-dish observations.

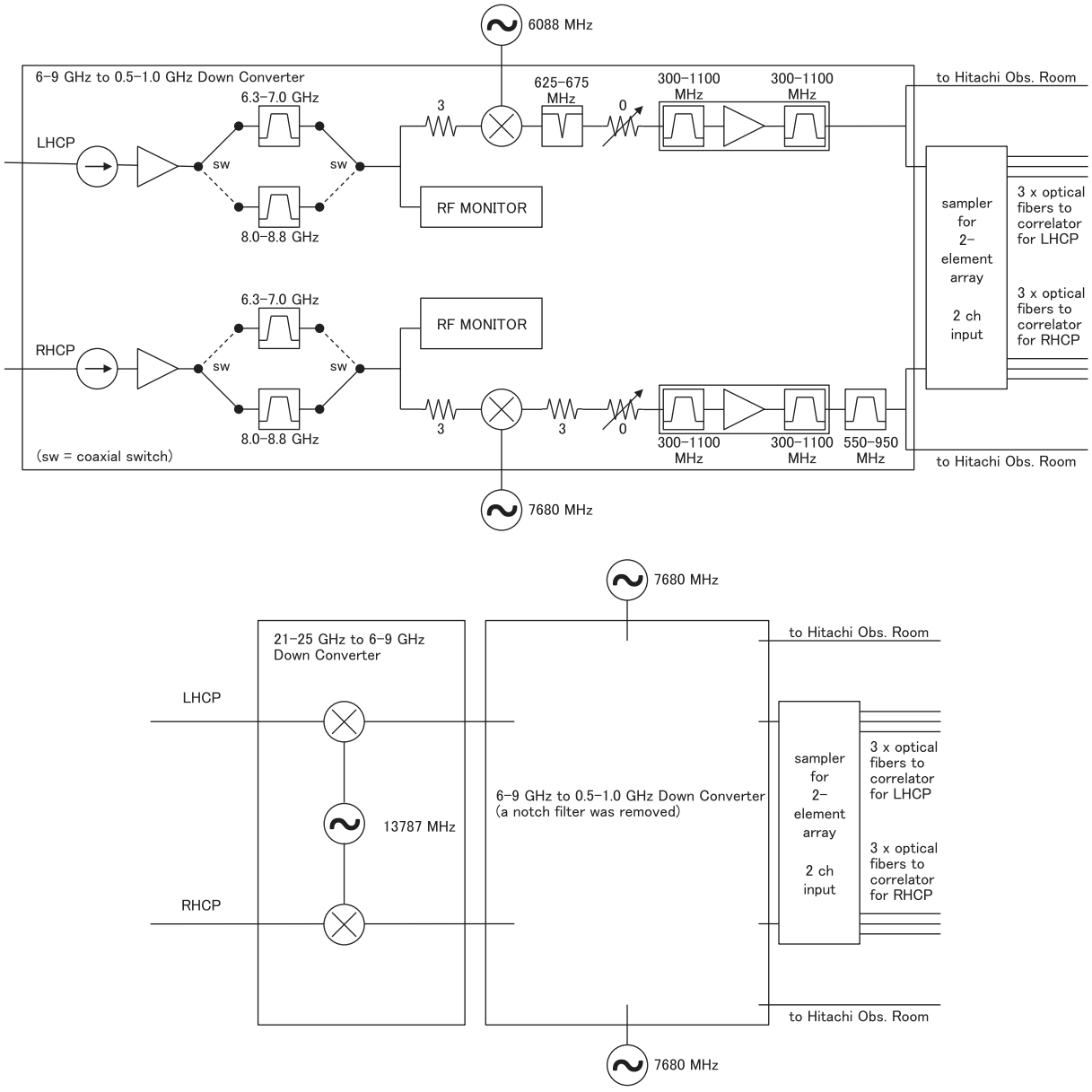

Fig. 6. (Top) Block diagram of the IF system for the low-frequency-band receiver. (Bottom) Block diagram of the IF system for the high-frequency-band receiver. The same down-converter from 6–9 GHz to 0.5–1.0 GHz for the low-frequency-band receiver is used, except that the local frequency is changed and the notch filter is removed.

For the Takahagi antenna, the same IF system as Hitachi is used except that the output after the division in the receiver cabin is sent to the observation room of the Hitachi antenna via an optical fiber link with a length of 500 m. We use an optical–electrical converter for the analog signal (Emcore WiBa). Data are sampled at the observation room of the Hitachi antenna.

For the high-frequency-band receiver, the 21–25 GHz output is down-converted to 6.3–8.8 GHz with a local frequency of 13787 MHz, and is then passed to the IF system for the low-frequency-band receiver. The local frequency is changed to 7680 MHz for both polarizations and the notch filter is removed. A block diagram of the IF system is shown in figure 6.

2.4 Samplers and recording system

For the VLBI observations, a 2 Gbps sampler (Digitallink ADS-1000+) is used (Koyama et al. 2008). We usually use a mode of 1 giga-samples per second with 2 bit sampling. The output of the ADS-1000+ is in the VLBI Standard Interface Hardware (VSI-H) format and is connected to OCTAVIA2

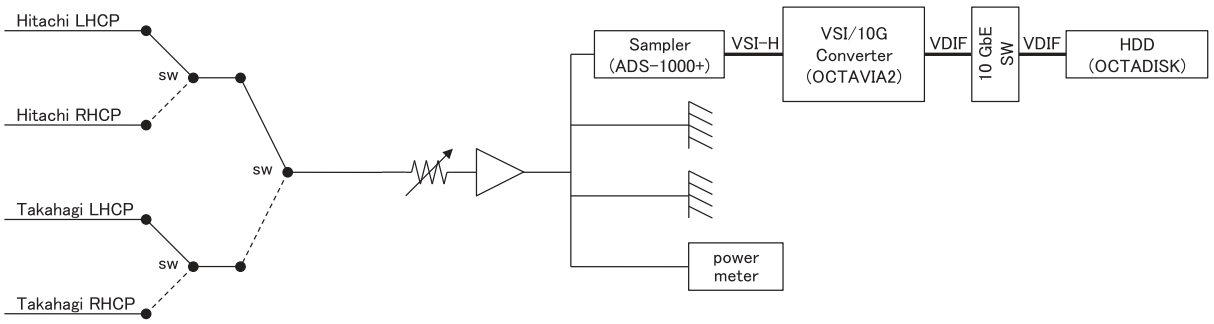

Fig. 7. Block diagram of the VLBI backend.

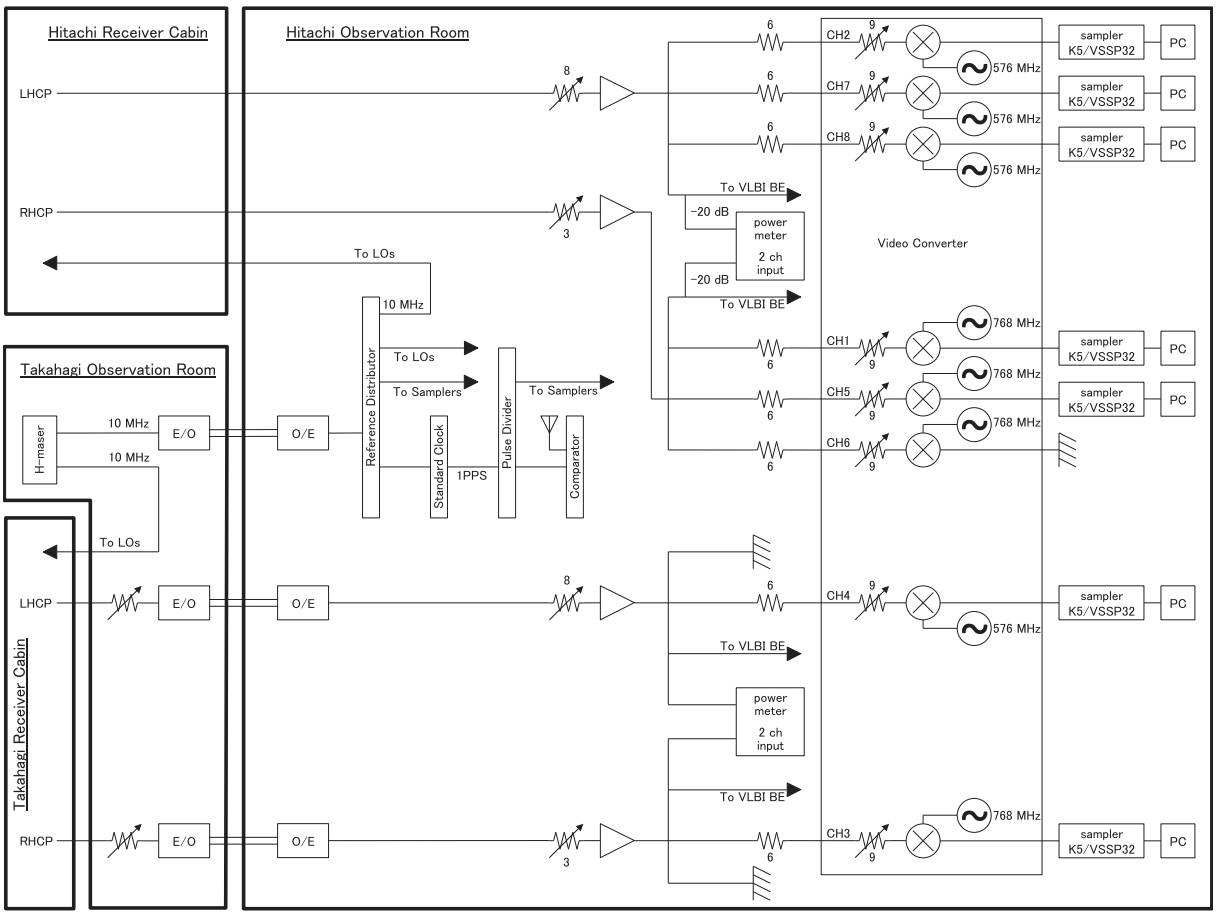

Fig. 8. Block diagram of the Ibaraki station.

(Elecs Industry) by a cable. OCTAVIA2 converts sampled data in VSI-H format into VLBI Data Interchange Format (VDIF) format and outputs on a 10 GbE port. The VDIF format data are stored in the OCTADISK (Elecs Industry). This can mount two disk packs of 24 TB each, and one disk pack can record 37.5 hr data at 2 Gbps. A block diagram of the VLBI back-end is shown in figure 7.

For the single-dish observations, a K5/VSSP32 (Nitsuki 9270) is used (Kondo et al. 2008). Seven sets of K5/VSSP32 are installed at Ibaraki station. We usually use the 64 Mbps mode (16 mega-samples per second with 4 bit sampling) for the observation of a methanol maser line at 6.7 GHz (see figure 8).

2.5 Reference and 1 PPS signals

A hydrogen maser (Anritsu SD1T03A) is installed in a constant temperature and constant humidity room at the Takahagi antenna. For the equipment in the Takahagi antenna, the reference signal is sent via coaxial cables. For the equipment in the Hitachi antenna, the reference signal of 10 MHz is sent to the observation room at the Hitachi antenna via

Table 1. Compact continuum sources used for the measurement of aperture efficiencies and beam patterns.

Name	Coordinates (J2000.0) RA (h m s), Dec (° ′ ″)	Size (″ × ″)	Flux density, 6.668 GHz (Jy)	Flux density, 8.400 GHz (Jy)	Variability
3C 48	01 37 41.300, +33 09 35.134	1.5 × 1.5	4.17*	3.33*	stable
3C 123	04 37 04.375, +29 40 13.819	23 × 5	11.76*	9.29*	stable
3C 161	06 27 10.111, −05 53 04.713	3 × 3	4.82*	3.79*	stable
3C 286	13 31 08.284, +30 30 32.940	1.5 × 1.5	6.10*	5.20*	stable
3C 84	03 19 48.161, +41 30 42.103	compact	∼20†	∼15†	variable
4C 39.25	09 27 03.014, +39 02 20.852	compact	∼12†	∼11†	variable
3C 273B	12 29 06.700, +02 03 08.598	compact	∼33†	∼28†	variable
OV 236	19 24 51.056, −29 14 30.117	compact	∼16†	∼12†	variable

*Flux densities were referred to Ott et al. (1994).

†Flux densities were estimated from the observations at Hitachi and Takahagi.

an optical fiber link with a length of 500 m. We use an optical–electrical converter for the analog signal (Emcore WiBa). Then the reference signal is distributed to the equipment in the Hitachi antenna via coaxial cables. In the observation room at the Hitachi antenna, 1 pulse per second (PPS) is generated by a standard clock (ECHO KEISOKUKI AQ-330D) from the 10 MHz reference signal and distributed to the equipment in the Hitachi antenna via coaxial cables. There is no equipment that needs 1 PPS in the Takahagi antenna. The time difference between the 1 PPS of the GPS and the 1 PPS of the standard clock is monitored by a GPS time comparator (ECHO KEISOKIKI GP-1100C).

Because the samplers for the Takahagi antenna are installed in the observation room at the Hitachi antenna, the data sampled by the samplers are signals that have been received 2.4 μs before the sampling— 2.4 μs is the time for the signals to travel the distance of 500 m within the optical fiber between Takahagi and Hitachi. Thus, a 2.4 μs offset is added to the time difference between the 1 PPS of GPS and the 1 PPS of the standard clock for the Takahagi data.

A block diagram of the Ibaraki station is shown in figure 8.

3 Resulting performance

3.1 Receiver temperature and system temperature

The receiver temperature, $T_{\rm rx}$, was measured by the Y-factor method with hot and cold loads. The receiver was cooled to ∼11 K. The measured receiver temperatures were ∼22 K, ∼15 K, and ∼30 K for 6 GHz, 8 GHz, and 22 GHz, respectively.

The system temperature including the atmosphere toward the zenith, $T^*_{\rm sys}$, was measured by the R-SKY method with hot load. The receiver was cooled to ∼11 K. The measured system temperatures for 6 GHz and 8 GHz were ∼30–40 K and ∼25–35 K, respectively. The optical depth of the atmosphere at 6 GHz and 8 GHz was ∼0.01 under good weather conditions, and ∼0.02 under bad weather conditions.

The system temperature for 22 GHz depends on the weather conditions and season. $T^*_{\rm sys}$ for 22 GHz in the winter and summer seasons were ∼40–100 K and ∼150–500 K, respectively. The optical depth of the atmosphere at 22 GHz was ∼0.03–0.2 in winter and ∼0.3–0.7 in summer.

3.2 Aperture efficiency, beam pattern, beam size, and their elevation dependences

The aperture efficiencies and beam patterns of the Hitachi and Takahagi antennas at 6 GHz and 8 GHz were measured by observations of the compact continuum sources with stable flux density (3C 123, 3C 286, 3C 161, 3C 48) and the others with variable flux density (3C 273B, 3C 84, OV 236, 4C 39.25). The latter sources are brighter than the former. The source list is given in table 1.

The total power of 6.3–7.0 GHz and 8.0–8.8 GHz was measured with a power meter. A 20′ × 20′ region was mapped by the on-the-fly method with a scan speed of 20 s per scan with a sampling rate of 5 Hz, resulting in a sampling separation of 0.′2 per sample, sufficiently dense sampling compared to the beam size of the antenna at these frequencies (∼3′–5′). The separation between scans was 1.′0. A linear fit to the power of both edges of the scan ($dAz = -10'$ and $dAz = +10'$) was subtracted from each ON measurement. Because the beam pattern is approximately Gaussian and the source size is much smaller than the beam size, we assumed an axisymmetric Gaussian distribution of the observed flux density,

$$P(dAz, dEl) = a \exp\left[-4\ln(2)\frac{(dAz-b)^2+(dEl-c)^2}{d^2}\right] + e, \qquad (1)$$

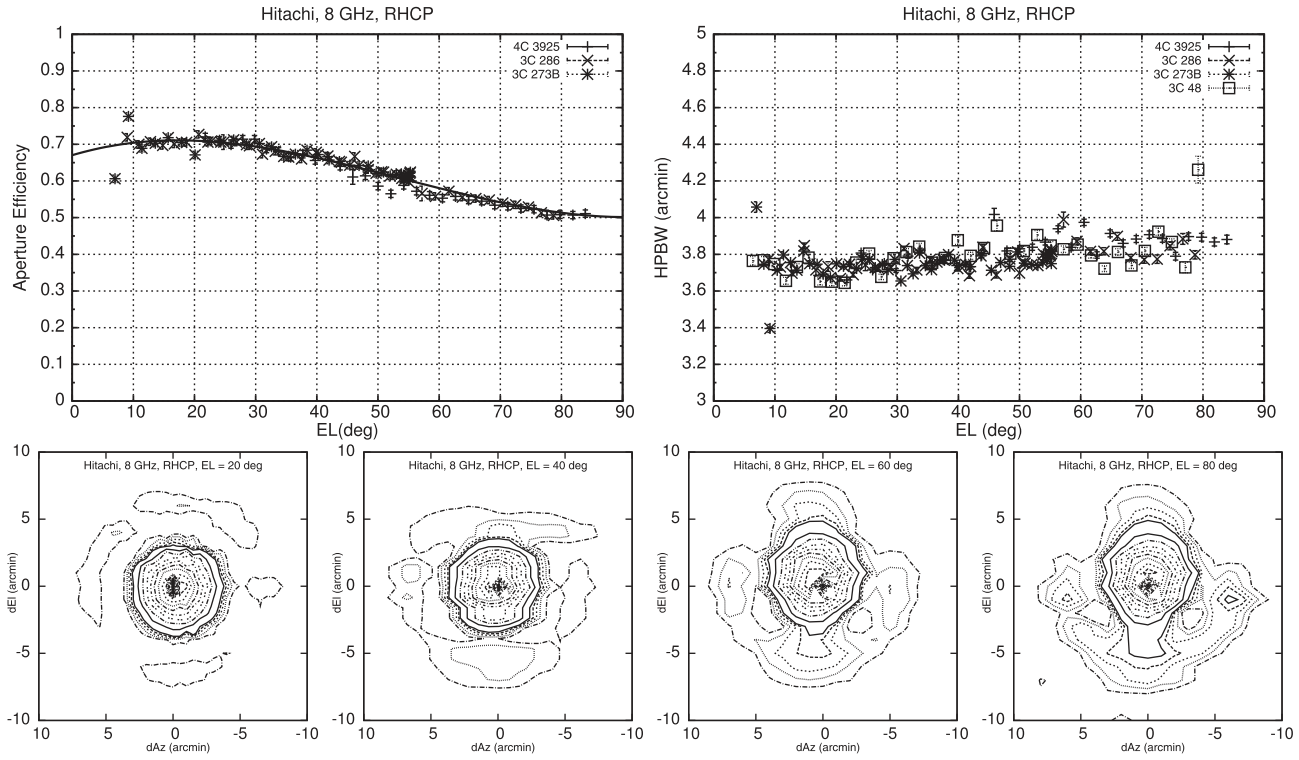

Fig. 9. (Top left) Elevation dependence of the aperture efficiency of the Hitachi antenna at 8 GHz in RHCP. (Top right) Elevation dependence of the HPBW of the Hitachi antenna at 8 GHz in RHCP. (Bottom) Beam patterns of the Hitachi antenna at 8 GHz in RHCP at $El = 20^\circ$, 40°, 60°, and 80°. The contour levels are 2%, 4%, 6%, 8%, 10%, 20%, 30%, 40%, 50%, 60%, 70%, 80%, 90%, and 100% of the peak intensity.

where a is the measured peak flux density $F_{\rm obs}(El)$ at the elevation angle El, and b and c are the pointing offsets in the Az and El directions, respectively. And d is the half-power beam width $\theta_{\rm HPBW}$, and e is the offset of the flux density due to bad ON–OFF subtraction caused by the fluctuation of the sky level.

For the sources with stable flux density F_ν (3C 48, 3C 123, 3C 161, and 3C 286), the aperture efficiency $\eta_{\rm A}(El)$ is calculated by

$$\eta_{\rm A}(El) = \frac{F_{\rm obs}(El)}{F_\nu}. \tag{2}$$

For the sources with variable flux density, we assumed the flux density F_ν of the day of observation by using $\eta_{\rm A}(El)$ estimated from the observations of sources with stable flux density, and then we calculated the elevation dependence of $\eta_{\rm A}(El)$.

Observations of the 8.4 GHz band for Hitachi were made on five days in 2011 June, October, and December. The observed sources were 3C 273B (variable), 4C 39.25 (variable), 3C 286 (stable), and 3C 48 (stable). The aperture efficiencies of Hitachi at 8.4 GHz have elevation dependence. The results of a fit with third-order polynomials are

$$\eta_{\rm H8L}(El) = 1.38 \times 10^{-6} El^3 - 2.28 \times 10^{-4} El^2 + 6.22 \times 10^{-3} El + 0.658 \tag{3}$$

and

$$\eta_{\rm H8R}(El) = 1.06 \times 10^{-6} El^3 - 1.72 \times 10^{-4} El^2 + 4.99 \times 10^{-3} El + 0.670, \tag{4}$$

where $\eta_{\rm H8L}$ and $\eta_{\rm H8R}$ denote the aperture efficiencies for LHCP and for RHCP of the Hitachi antenna at 8.4 GHz, respectively.

The main beam has an axisymmetric Gaussian distribution with HPBW of $\sim 3'.8$ with a slight elevation dependence. For low elevations of 20° and 40°, an axisymmetric side-lobe is apparent with a level of $\sim$4%. For high elevations of 60° and 80°, the shape of the side-lobe changes and the side-lobe level reaches $\sim$10%, which may result either from the deformation of the main dish or from the displacement of the subreflector due to gravity, because the antenna is designed to have best performance at the elevation angle of 35°. See figure 9.

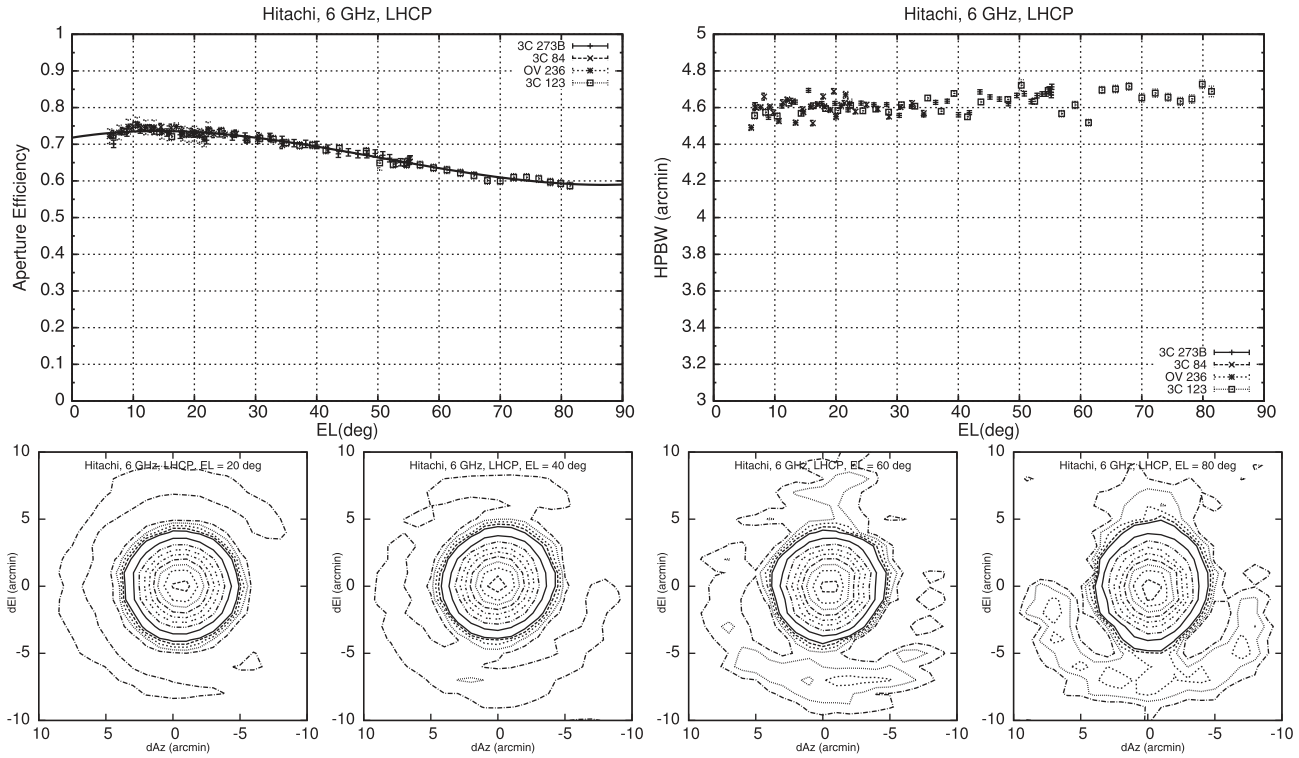

Fig. 10. Same as in figure 9, but for the Hitachi antenna at 6 GHz in LHCP.

Observations of the 6.7 GHz band for Hitachi were made on two days in 2011 December; the sources observed were 3C 273B (variable), OV 236 (variable), 3C 84 (variable), and 3C 123 (stable). The aperture efficiencies of Hitachi at 6.7 GHz have elevation dependence. The results of a fit with third-order polynomials are

$$\eta_{\mathrm{H6L}}(El) = 7.51 \times 10^{-7} El^3 - 1.14 \times 10^{-4} El^2 + 2.75 \times 10^{-3} El + 0.718 \quad (5)$$

and

$$\eta_{\mathrm{H6R}}(El) = 5.56 \times 10^{-7} El^3 - 8.87 \times 10^{-5} El^2 + 2.27 \times 10^{-3} El + 0.706, \quad (6)$$

where η_{H6L} and η_{H6R} denote the aperture efficiencies for LHCP and RHCP of the Hitachi antenna at 6.7 GHz, respectively.

The main beam has an axisymmetric Gaussian distribution with HPBW of $\sim 4\farcm6$ with slight elevation dependence. The beam patterns have the same tendency as for 8.4 GHz: For low elevations of 20° and 40°, an axisymmetric side-lobe is apparent with a level of ∼3%. For high elevations of 60° and 80°, the shape of the side-lobe changes and the side-lobe level reaches ∼6%. See figure 10.

Observations of the 8.4 GHz band for Takahagi were made on two days in 2012 July; the observed sources were 3C 273B (variable), 3C 123 (stable), and 3C 84 (variable). The aperture efficiency of Takahagi at 8.4 GHz has elevation dependence. The result of a fit with third-order polynomials is

$$\eta_{\mathrm{T8R}}(El) = 4.53 \times 10^{-7} El^3 - 8.13 \times 10^{-5} El^2 + 3.98 \times 10^{-3} El + 0.535, \quad (7)$$

where η_{T8R} denotes the aperture efficiency for RHCP of the Takahagi antenna at 8.4 GHz.

The main beam has an axisymmetric Gaussian distribution with HPBW of $\sim 3\farcm7$ with slight elevation dependence. A nearly axis-symmetric side-lobe with a level of ∼4% is apparent at any elevation angle. See figure 11.

In order to measure the side-lobe pattern down to 0.1% of the peak level, we observed the strong methanol maser source G09.621+0.196. By offsetting the antenna in the azimuth direction by angles of 1′, 2′, . . . , 60′, we measured the peak flux density of G09.621+0.196 for each offset angle. Observations were made on 2014 March 20–21. The results (figure 12) show that the side-lobe intensity is between −20 dB and −30 dB at offset angles of 10′–20′, between −25 dB and −35 dB at 20′–30′, and between −30 dB and −40 dB at 30′–60′.

The measured parameters and the derived system equivalent flux densities (SEFD) are summarized in table 2.

Table 2. Measured and derived parameters of the Hitachi and Takahagi antennas.

Frequency band (GHz)	T_{sys} (K)	Optical depth	Aperture efficiency	SEFD (Jy)	HPBW (′)	Conditions
6	30	0.01	0.6–0.75	140–170	4.5–4.7	good weather
6	40	0.02	0.6–0.75	180–230	4.5–4.7	bad weather
8	25	0.01	0.5–0.7	120–170	3.6–4.0	good weather
8	35	0.02	0.5–0.7	170–240	3.6–4.0	bad weather
22	40	0.03	0.3*	460	not measured	winter, good weather
22	100	0.2	0.3*	1100	not measured	winter, bad weather
22	150	0.3	0.3*	1700	not measured	summer, good weather
22	500	0.7	0.3*	5700	not measured	summer, bad weather

*Preliminary results.

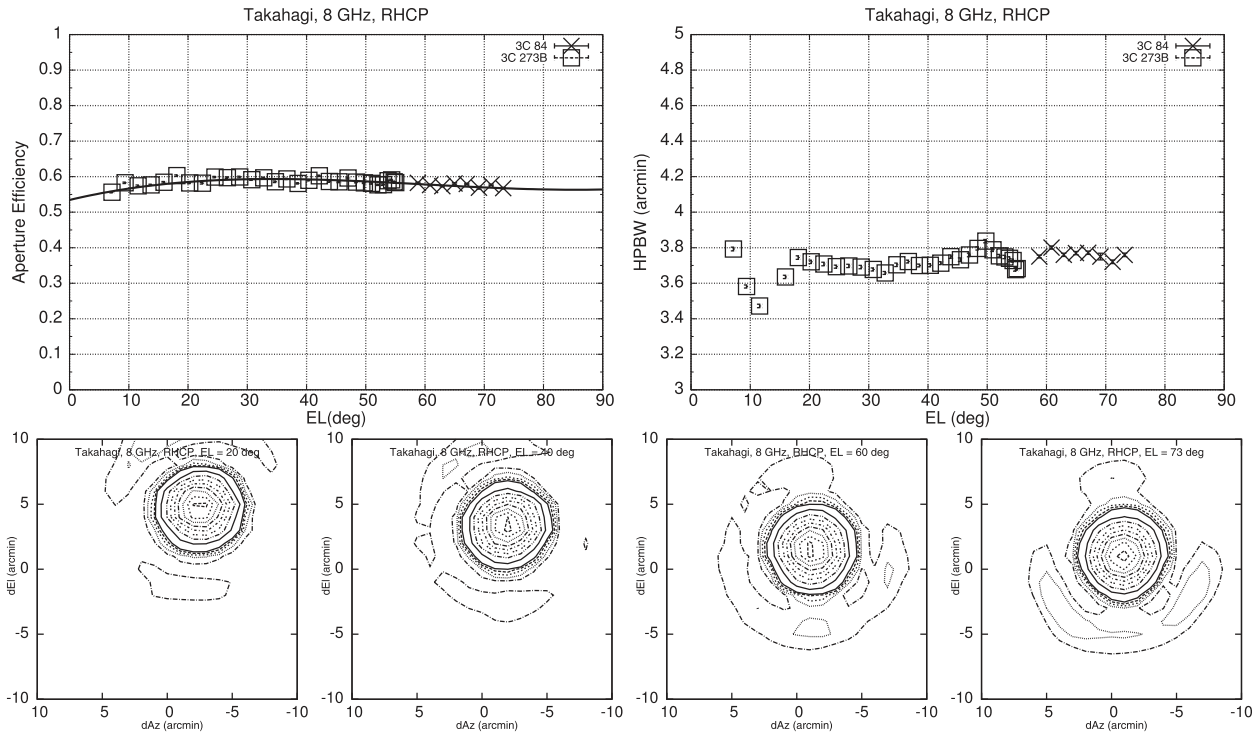

Fig. 11. (Top left) Elevation dependence of the aperture efficiency of the Takahagi antenna at 8 GHz in RHCP. (Top right) Elevation dependence of the HPBW of the Takahagi antenna at 8 GHz in RHCP. (Bottom) Beam patterns of the Takahagi antenna at 8 GHz in RHCP at $El = 20°$, $40°$, $60°$, and $73°$. The contour levels are 2%, 4%, 6%, 8%, 10%, 20%, 30%, 40%, 50%, 60%, 70%, 80%, 90%, and 100% of the peak intensity.

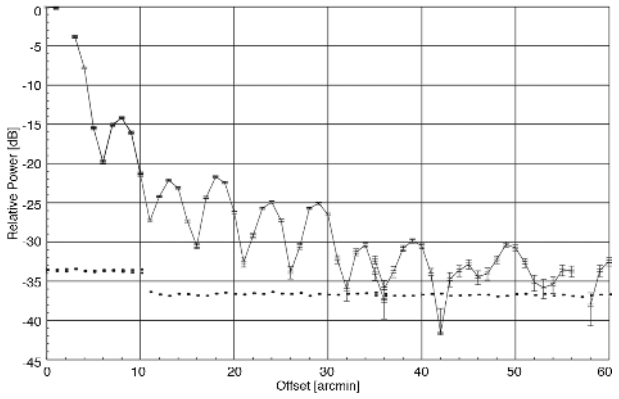

Fig. 12. Side-lobe pattern of the Hitachi antenna at 6.7 GHz.

3.3 Telescope pointing

Pointing offsets in the azimuth and elevation directions [$dX \equiv \cos(El)dAz$, dEl] were determined based on nine-point cross-scans toward pointlike strong continuum sources with known position. For each measurement, cross-scans of about 50–100 sets were made over all celestial hemispheres for 2–4 d, mainly at night.

The observed pointing offsets were parameterized with the model described in the equation below. These parameters ($A1$–$A12$) were determined with a least-squares fit. We added the terms in periods of 180° for azimuth [$\sin(2Az)$

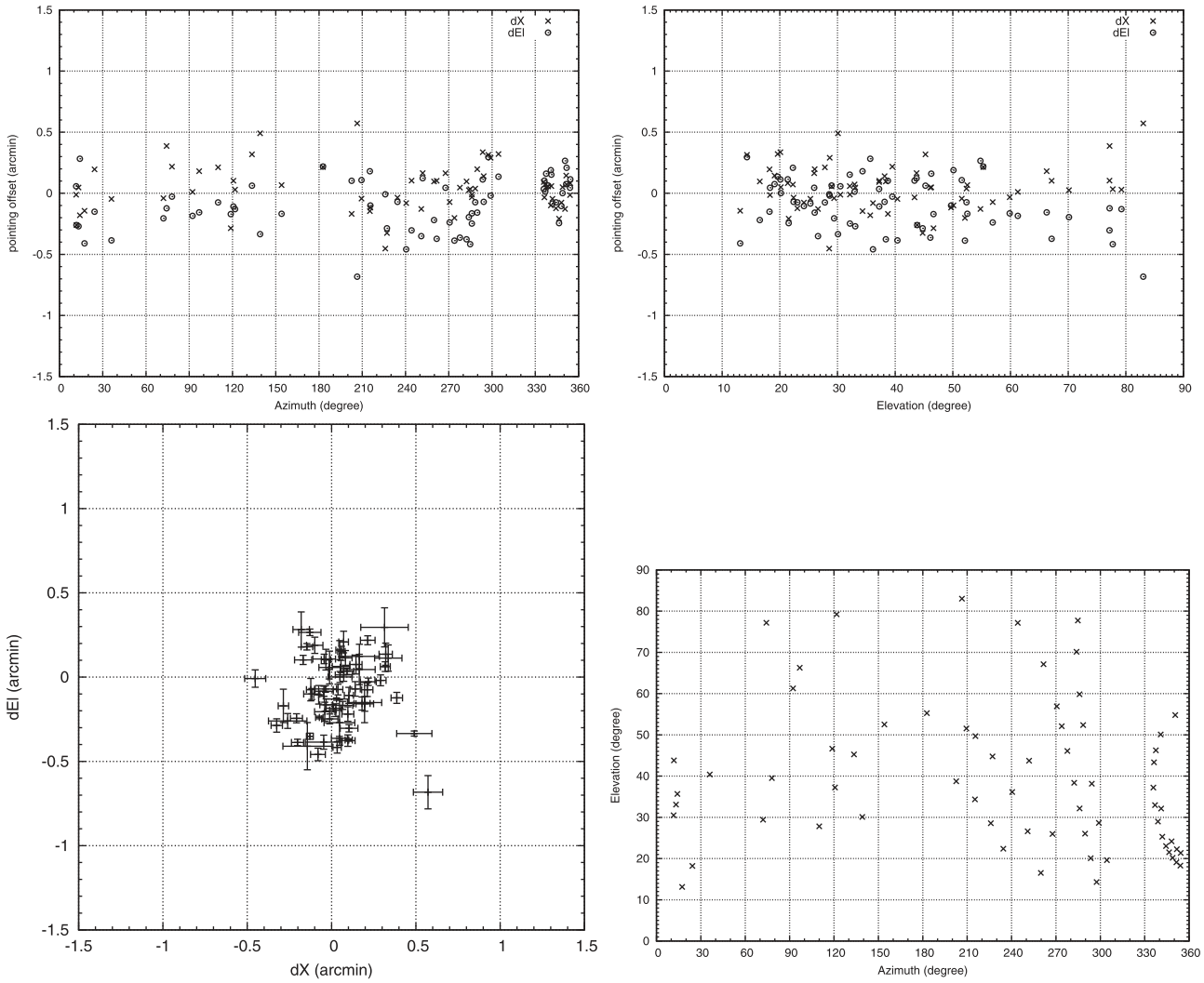

Fig. 13. Pointing residuals for the Hitachi antenna at 8 GHz. (Top left) Relation of the azimuth to the pointing residuals in azimuth and elevation. (Top right) Relation of the elevation to the pointing residuals in azimuth and elevation. (Bottom left) Relation of the pointing residuals in azimuth to those in elevation. (Bottom-right) Positions on the celestial sphere of the objects that were observed in the pointing measurements.

and $\cos(2Az)$] to the model equation, in order to improve pointing accuracy.

$$dX = A1\cos(El) + A3\cos(Az)\sin(El) - A4\sin(Az)\sin(El) + A5\sin(El) + A7 + A9\sin(2Az) + A10\cos(2Az), \quad (8)$$

$$dEl = A2 - A3\sin(Az) - A4\cos(Az) + A6\cos(El) + A8\sin(El) + A11\sin(2Az) + A12\cos(2Az), \quad (9)$$

where *A1* is the *Az* encoder zero offset; *A2* is the *El* encoder zero offset; *A3* is the inclination of the *Az* axis to the east–west direction; *A4* is the inclination of the *Az* axis to the north–south direction; *A5* is the nonorthgonality between the *Az* and *El* axes; *A7* is the collimation error (nonorthogonality of the radio beam axis and *El* axis); *A6* and *A8* are the corrections for gravitational bending; *A9–A12* are coefficients for the 180° period term.

Measurements for the Hitachi antenna at 8 GHz were executed on 2012 April 12. We achieved a pointing accuracy of 0.″27, which is smaller than 1/10 of the beam size in the *C* and *X* bands (∼4.″6 and ∼3.″8, respectively), and enough for science observations in the *C* and *X* bands. See figure 13.

Measurements for the Takahagi antenna at 8 GHz were executed on 2012 June 16. We achieved a pointing accuracy of 0.″63, which is 1–2 times larger than 1/10 of the beam size in the *C* and *X* bands, and thus further improvement is needed. See figure 14.

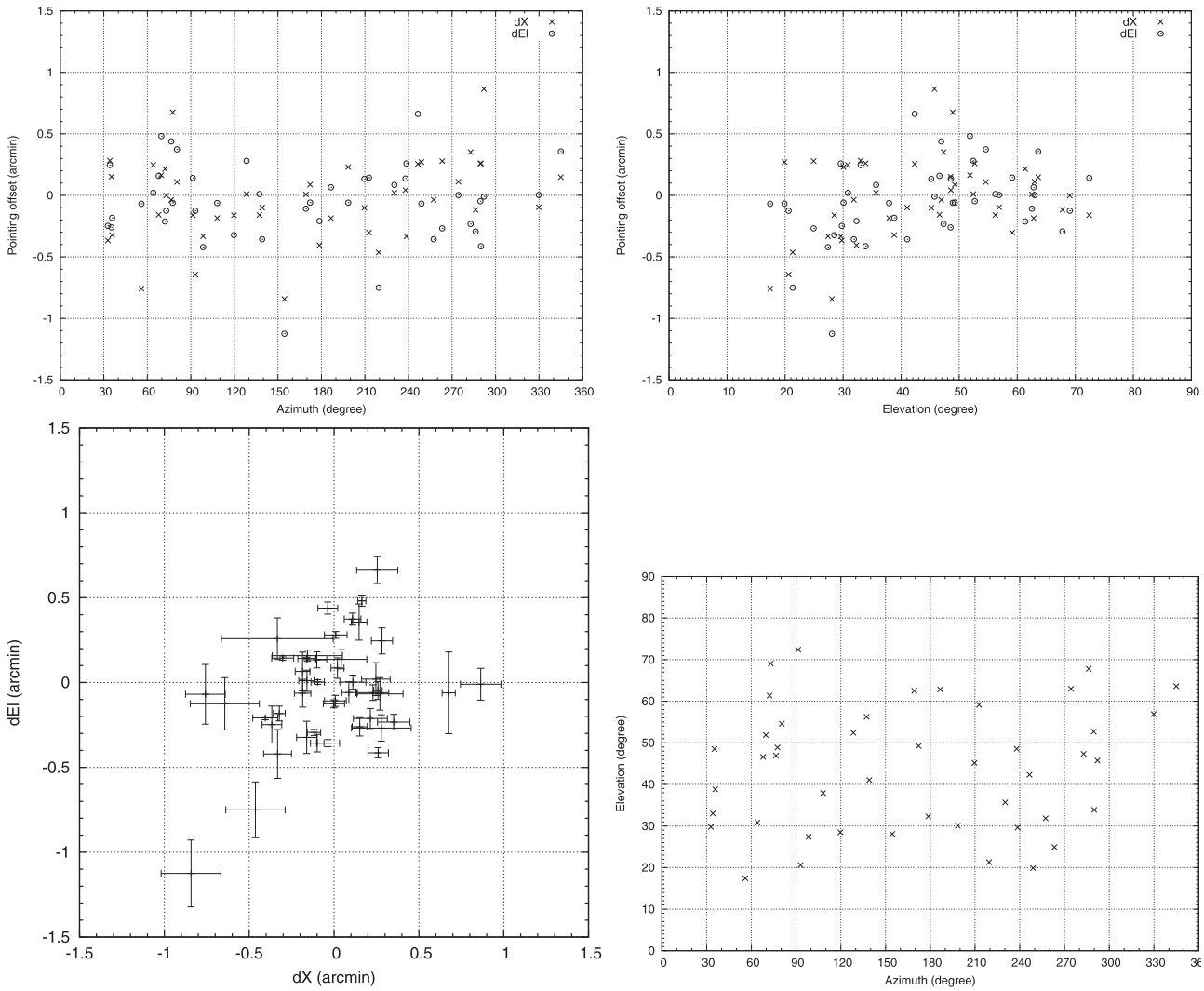

Fig. 14. Same as in figure 13, but for the Takahagi antenna at 8 GHz.

3.4 Antenna coordinates

The positions of the antennas were measured in 2010 September, 2011 June, 2012 September, and 2015 November with geodetic GPS receivers. The local ties between GPS observation points and antennas were carried out with a total station. The results are summarized in table 3. Note that the post-seismic movement of the antennas after the 2011 earthquake off the Pacific coast of Tohoku can be seen.

4 Observations

4.1 VLBI observations

The first scientific VLBI observations with the Hitachi antenna were executed in 2010 August with four VERA stations and the Shanghai 25 m telescope at 6.7 GHz observing methanol masers. Details of the observations and the initial results have already been published (Fujisawa et al. 2014a; Sugiyama et al. 2016). Fringes have been successfully detected toward both the methanol maser sources and the continuum sources (figure 15).

Figure 16 presents the autocorrelation function of the data obtained by six antennas (four VERA stations, Shanghai 25 m, and Hitachi 32 m) on 2010 August 29. Note that the signal-to-noise ratio of the spectrum obtained at Hitachi is the highest, showing good performance. This is thanks to the large collecting area and the low system temperature of the Hitachi antenna.

In addition to the normal JVN mode, i.e., one of the Hitachi and Takahagi antennas joins the VLBI observation, the following two observation modes are under development. One is to use the Hitachi and Takahagi antennas as a two-element interferometer. In this interferometer mode, the flux of the target can easily be measured without

Table 3. Antenna coordinates.

Antenna	Period	*X* (m)	*Y* (m)	*Z* (m)
Hitachi	2010 Sep	−3961787.684	3243598.964	3790598.229
Hitachi	2011 Jun	−3961788.613	3243597.622	3790597.760
Hitachi	2012 Sep	−3961788.796	3243597.525	3790597.709
Hitachi	2015 Nov	−3961788.974	3243597.492	3790597.692
Takahagi	2010 Sep	−3961880.535	3243373.951	3790687.986
Takahagi	2011 Jun	−3961881.464	3243372.610	3790687.517
Takahagi	2012 Sep	−3961881.647	3243372.513	3790687.466
Takahagi	2015 Nov	−3961881.825	3243372.480	3790687.449
Distance between the two antennas: 259.439 m				

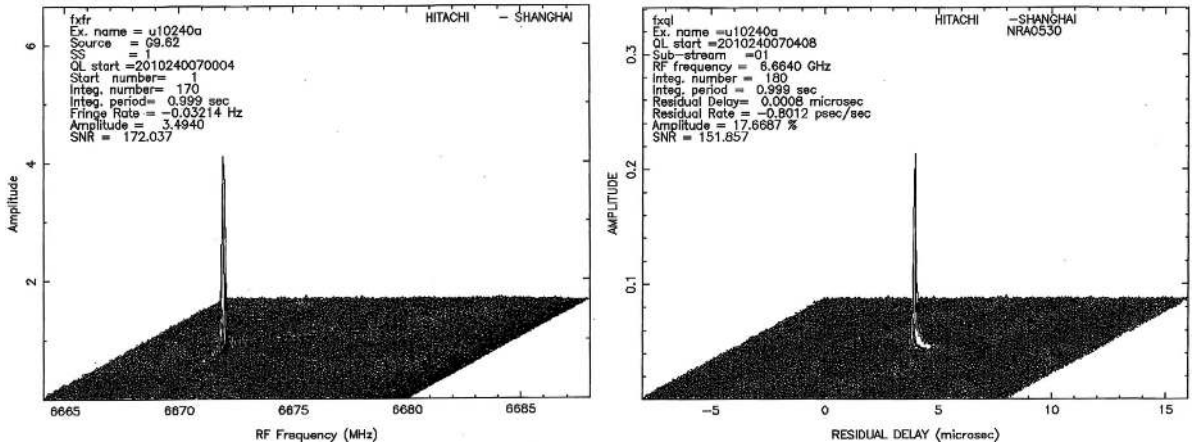

Fig. 15. (Left) Plot of the fringe between Shanghai 25 m and Hitachi 32 m toward the methanol maser source G09.621+0.196 observed on 2010 August 28. (Right) Plot of the fringe between Shanghai 25 m and Hitachi 32 m toward the continuum source NRAO 530 observed on 2010 August 28.

switching the antenna between the target and the blank sky. A problem was found during the initial test that the correlated amplitude and phase varied sinusoidally (Kako et al. 2015). By installing band-pass filters, the problem was solved (figure 17). The other observation mode is a two-beam mode that is achieved when one of the Hitachi or Takahagi antennas points to the target and the other points to a calibrator. Details of these two modes will appear in a separate paper.

4.2 Single-dish observations of methanol masers at 6.7 GHz

Methanol masers at 6.7 GHz are associated only with massive-star-forming regions, and thus can be used as good tracers for massive-star formation. Up to now, more than 1000 6.7 GHz methanol masers have been found (Pandian et al. 2007; Xu et al. 2009; Caswell et al. 2010, 2011; Green et al. 2010, 2012; Breen et al. 2015). At least 242 out of 320 show variability (Caswell et al. 1995; Szymczak et al. 2000; Goedhart et al. 2004). Twenty sources show periodic variability with periods of 29.5–668 days (Goedhart et al. 2003, 2004, 2007, 2009; Araya et al. 2010; Szymczak et al. 2011, 2014, 2015; Fujisawa et al. 2014b; Maswanganye et al. 2015, 2016), and two show strong variability: the flux density of G33.641+0.228 became a few to few tens times that in a quiescent period within one day, and such phenomena were detected five times during the 294 days of observations performed from 2009 to 2012 (Fujisawa et al. 2012, 2014c); also, for G351.42+00.64 (NGC 6334 F) the flux density became $\geq$250 times that in a quiescent period within two months (Goedhart et al. 2004).

Several mechanisms are suggested to explain such periodic variability (e.g., Goedhart et al. 2008); however, a unified picture is not obtained. Recently, Inayoshi et al. (2013) suggested periodic variability due to pulsating instability of massive stars, and also showed that the period–luminosity relation will be obtained.

In order to obtain more samples of burstlike variability and periodic variability, especially with period of 30–120 days because samples with these periods are lacking in the previous studies, from 2012 December we have been monitoring observations of more than four hundred 6.7 GHz methanol masers, i.e., all known 6.7 GHz methanol masers that can be observed at Ibaraki. Up to now, we have detected more than ten new sources with

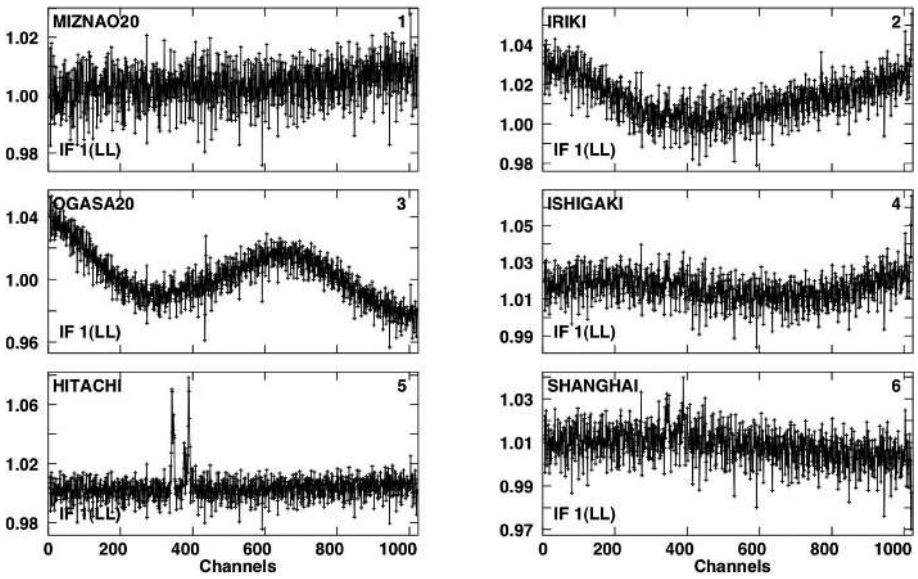

Fig. 16. Comparison of the autocorrelation function of the 6.7 GHz methanol maser emission viewed toward G28.83−0.25 obtained by four VERA antennas, Shanghai 25 m, and Hitachi 32 m. The observations were made on 2010 August 29.

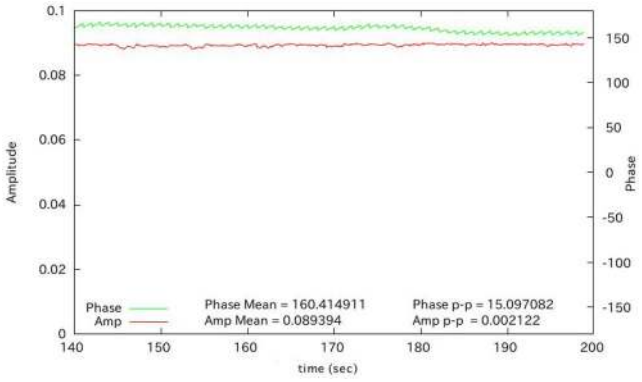

Fig. 17. Correlated amplitude and phase of the Hitachi and Takahagi antennas toward 3C 273B. The observed frequency range is 8192–8704 MHz. (Color online)

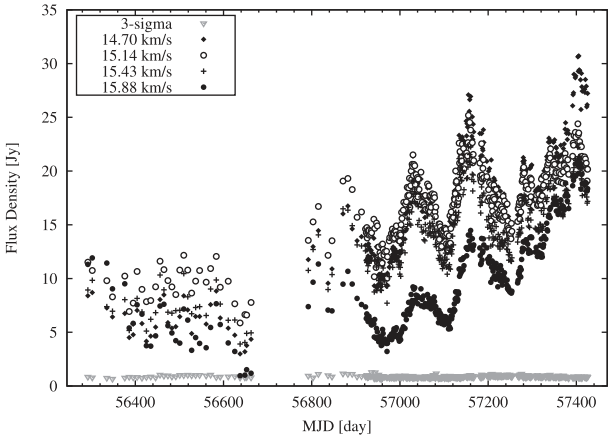

Fig. 18. Time variations of the flux density of each velocity component of the methanol maser source G196.45−01.67 observed at Hitachi.

periodic variability and one new source where the flux density became ≥10 times higher within a few days. Figure 18 shows the time variations of the flux density of each velocity component of the methanol maser source G196.45−01.67. The source had been found to show a periodic flux variability with a period of 668 days (Goedhart et al. 2004). In our observations, we found a new period of ∼130 days toward all of the four velocity components. Details of the observations will be presented in separate papers.

5 Summary

Former satellite communication antennas were upgraded to become the Hitachi and Takahagi 32 m radio telescopes at 6, 8, and 22 GHz. We have developed receiver systems, IF systems, back-end systems (including samplers and recorders), and reference systems. We have measured the performance of the antennas. The system temperature including the atmosphere toward the zenith, $T^*_{\rm sys}$, is measured to be ∼30–40 K and ∼25–35 K for 6 GHz and 8 GHz, respectively. $T^*_{\rm sys}$ for 22 GHz is measured to be ∼40–100 K and ∼150–500 K for the winter and summer seasons, respectively. The aperture efficiency is 55%–75% for Hitachi at 6 GHz and 8 GHz, and 55%–65% for Takahagi at 8 GHz. The beam sizes are ∼4.′6 and ∼3.′8 at 6 GHz and 8 GHz, respectively. Side-lobe level is less than 3%–4% at 6 and 8 GHz. Pointing accuracy was measured to be better than ∼0.′3 for Hitachi and ∼0.′6 for Takahagi. We succeeded in VLBI observations in 2010 August, indicating the good performance of the antenna. We started single-dish monitoring observations of 6.7 GHz methanol

maser sources in 2012 December. We found several new sources showing short-term periodic variation of the flux density.

Acknowledgments

The authors would like to thank Yoshiyuki Hoshi, Misato Takizawa, Jun Kurihashi, Tomoaki Tanaka, Tomohiko Mori, Kohei Matsumoto, Junki Kizawa, Kazuki Tokuda, and Naoko Furukawa for their contributions to this project. Thanks are also due to the staff of the Mizusawa VLBI observatory and the members of the JVN team for various kinds of support and observational assistance. This work was financially supported in part by a Grant-in-Aid for Scientific Research (KAKENHI) from Japan Society for the Promotion of Science (JSPS), No. 24340034. We are grateful to NICT for the use of the correlation software.

References

Araya, E. D., Hofner, P., Goss, W. M., Kurtz, S., Richards, A. M. S., Linz, H., Olmi, L., & Sewiło, M. 2010, ApJ, 717, L133
Breen, S. L., et al. 2015, MNRAS, 450, 4109
Caswell, J. L., et al. 2010, MNRAS, 404, 1029
Caswell, J. L., et al. 2011, MNRAS, 417, 1964
Caswell, J. L., Vaile, R. A., Ellingsen, S. P., Whiteoak, J. B., & Norris, R. P. 1995, MNRAS, 272, 96
Chen, M. H., & Tsandoulas, G. N. 1973, IEEE Trans. Antennas Propag., 21, 389
Cresci, L., Ciappi, L., Nesti, R., Palagi, F., & Panella, D. 2002, Arcetri Technical Report, 6/2002
Fujisawa, K., et al. 2012, PASJ, 64, 17
Fujisawa, K., et al. 2014a, PASJ, 66, 31
Fujisawa, K., et al. 2014b, PASJ, 66, 78
Fujisawa, K., et al. 2014c, PASJ, 66, 109
Goedhart, S., Gaylard, M. J., & van der Walt, D. J. 2003, MNRAS, 339, 33
Goedhart, S., Gaylard, M. J., & van der Walt, D. J. 2004, MNRAS, 355, 553
Goedhart, S., Gaylard, M. J., & van der Walt, D. J. 2007, in IAU Symp. 242, Astrophysical Masers and their Environments, ed. J. M. Capman & W. A. Baan (Cambridge: Cambridge University Press), 97
Goedhart, S., Gaylard, M., van der Walt, J., & Elitzur, M. 2008, in ASP Conf. Ser., 387, Massive Star Formation: Observations Confront Theory, ed. H. Beuther et al. (San Francisco: ASP), 124
Goedhart, S., Langa, M. C., Gaylard, M. J., & van der Walt, D. J. 2009, MNRAS, 398, 995
Green, J. A., et al. 2010, MNRAS, 409, 913
Green, J. A., et al. 2012, MNRAS, 420, 3108
Inayoshi, K., Sugiyama, K., Hosokawa, T., Motogi, K., & Tanaka, K. E. I. 2013, ApJ, 769, L20
Kaiden, M., Matsumoto, K., Kimura, K., Ogawa, H., & Asayama, S. 2010, IEICE Trans. Electron., J93-C, 339 (in Japanese)
Kako, R., Momose, M., Yonekura, Y., & Sugiyama, K. 2015, IVS NICT-TDC News No. 35, 14
Kondo, T., Koyama, Y., Ichikawa, R., Sekido, M., Kawai, E., & Kimura, M. 2008, J. Geod. Soc. Jpn, 54, 233
Koyama, Y., Kondo, T., Sekido, M., Nakajima, J., Kimura, M., & Takeuchi, H. 2008, J. Geod. Soc. Jpn, 54, 249
Maswanganye, J. P., Gaylard, M. J., Goedhart, S., van der Walt, D. J., & Booth, R. S. 2015, MNRAS, 446, 2730
Maswanganye, J. P., van der Walt, D. J., Goedhart, S., & Gaylard, M. J. 2016, MNRAS, 456, 4335
Ott, M., Witzel, A., Quirrenbach, A., Krichbaum, T. P., Standke, K. J., Schalinski, C. J., & Hummel, C. A. 1994, A&A, 284, 331
Pandian, J. D., Goldsmith, P. F., & Deshpande, A. A. 2007, ApJ, 656, 255
Sugiyama, K., et al. 2016, PASJ, 68, 72
Szymczak, M., Hrynek, G., & Kus, A. J. 2000, A&AS, 143, 269
Szymczak, M., Wolak, P., & Bartkiewicz, A. 2014, MNRAS, 439, 407
Szymczak, M., Wolak, P., & Bartkiewicz, A. 2015, MNRAS, 448, 2284
Szymczak, M., Wolak, P., Bartkiewicz, A., & van Langevelde, H. J. 2011, A&A, 531, L3
Xu, Y., Voronkov, M. A., Pandian, J. D., Li, J. J., Sobolev, A. M., Brunthaler, A., Ritter, B., & Menten, K. M. 2009, A&A, 507, 1117